Journal of Process Control 78 (2019) 34–44

Contents lists available at ScienceDirect

Journal of Process Control

journal homepage: www.elsevier.com/locate/jprocont

Robustness analysis of a nucleic acid controller for a dynamic biomolecular process using the structured singular value

Nuno M.G. Paulino[a,*], Mathias Foo[b], Jongmin Kim[c], Declan G. Bates[a]

[a] Warwick Integrative Synthetic Biology Centre, School of Engineering, University of Warwick, Coventry CV4 7AL, UK
[b] School of Mechanical, Aerospace and Automotive Engineering, Coventry University, Coventry CV1 5FB, UK
[c] Department of Integrative Biosciences and Biotechnology, Pohang University of Science and Technology (POSTECH), Pohang, Gyeongbuk, 37673, South Korea

ARTICLE INFO

Article history:
Received 13 December 2018
Received in revised form 19 February 2019
Accepted 25 February 2019

Keywords:
Synthetic biology
Chemical reaction networks
Nonlinear systems
Robustness
Systems and control theory

ABSTRACT

In the field of synthetic biology, theoretical frameworks and software tools are now available that allow control systems represented as chemical reaction networks to be translated directly into nucleic acid-based chemistry, and hence implement embedded control circuitry for biomolecular processes. However, the development of tools for analysing the robustness of such controllers is still in its infancy. An interesting feature of such control circuits is that, although the transfer function of a linear system can be easily implemented via a chemical network of catalysis, degradation and annihilation reactions, this introduces additional nonlinear dynamics, due to the annihilation kinetics. We exemplify this problem for a dynamical biomolecular feedback system, and demonstrate how the structured singular value (μ) analysis framework can be extended to rigorously analyse the robustness of this class of system. We show that parametric uncertainty in the system affects the location of its equilibrium, and that this must be taken into account in the analysis. We also show that the parameterisation of the system can be scaled for experimental feasibility without affecting its robustness properties, and that a statistical analysis via Monte Carlo simulation fails to uncover the worst-case uncertainty combination found by μ-analysis.

1. Introduction

With the recent increase in the scope and industrial potential of synthetic control systems for biochemical processes, it is appealing to try to exploit the long-established tools and techniques of linear control theory for the synthesis and analysis of biomolecular controllers. This goal requires the development of molecular circuits that are suitable for different biological contexts, and are capable of implementing analog computations [1] or the frequency descriptions underlying [2] linear feedback. With their extensive computational capabilities [3,4], chemical reaction networks (CRNs) provide a convenient representation for implementing elementary arithmetic operations [5] or the computation of polynomials [6], using any chemical system with mass-action kinetics. They also provide an appropriate level of abstraction for designing complex circuits [7], and integrating the different elements necessary to build linear feedback control systems [8].

One challenge in the representation of linear negative feedback control in this context is the positivity of the CRNs, where the subtraction modules are usually one sided [5,9], and compute only the positive control error. An alternative is the adoption of CRNs for dual-rail computation [8,10], to extend the signals into the real domain and enable negative control errors. Another challenge in terms of implementation is retroactivity, where the CRNs must preserve the modularity of the elementary CRNs when interconnected, either through insulation devices [11] or by design [12]. The methodology from [8] facilitates the implementation of embedded synthetic controllers due to the fact that linear operations (e.g., integration, sum, gain, etc) can be implemented with networks of elementary chemical reactions, i.e. catalysis, degradation and annihilation. Also, each signal in the system is represented as the difference between two species concentrations, employing dual-rail computations that yield a two-sided subtraction. This approach was exploited and extended in [13] to define configurable primitives, which can then be combined to realise any transfer function. The resulting CRNs can then be mapped into chemistry based on deoxyribonucleic acid (DNA) strands, through programmable *DNA*

* Corresponding author.
E-mail addresses: N.Paulino@warwick.ac.uk (N.M.G. Paulino), Mathias.Foo@coventry.ac.uk (M. Foo), jongmin.kim@postech.ac.kr (J. Kim), D.Bates@warwick.ac.uk (D.G. Bates).

https://doi.org/10.1016/j.jprocont.2019.02.009
0959-1524/

strand displacement (DSD) reactions [14,15]. The sequence design of DNA species provides a mechanism to tag species and program the affinities in each reaction [16,17]. It preserves modularity and can be scaled up to a very large number of chemical species [18]. The available mapping between transfer functions, CRNs and DSD reactions makes straighforward the use of classical control theory in the synthesis and implementation of biomolecular control systems, [8,17,19,20].

A significant complicating factor with the above approach is that even if the starting point is a prescribed linear system, the corresponding CRN representation introduces annihilation reactions whose dynamics are nonlinear [21]. These reactions typically operate on much faster time-scales than the rest of the system, and are used to keep the concentrations of the different chemical species required to a minimum. The mass action kinetics of these reactions introduce nonlinear dynamics, which are not observed in the I/O linear system, but are essential in determining its internal stability and positive equilibrium. In this work, we consider the impact of these issues on the analysis of the robust stability properties of a prototype biomolecular reference tracking controller for a single-input/single-output (SISO) dynamical process. Using its CRN representation, we express the dynamics of the system in their positive natural coordinates - species concentrations - where the nonlinear dynamics are observable. In the stability analysis, we must account for inevitable uncertainty in the values of the reaction rates actually implemented in the biochemical network [22]. Our approach is similar to [23], where the nonlinear dynamics in the presence of real parameteric uncertainties are analysed locally, and a stability margin is defined and numerically computed for the linearisation around an equilibrium of the system. We show how a rigorous analysis of the robust stability properties of the controller can be carried out using the structured singular value (SSV or μ) framework [24,25].

The dynamics are linearised around a fixed point, at the equilibrium of the system, to represent the uncertain system with a Linear Fractional Transformation (LFT) [26]. The fixed point can change with parameteric variation, and the *movement of the equilibrium* [27] with the uncertainty is included in the LFT. In our case, we do not have an analytical solution for this dependency, and the equilibrium variation is approximated by a function which can be represented as an LFT. The μ framework can then be applied to the LFT representation of the uncertain system, e.g., [28] applies the SSV with the LFT description to assess how far the system is from bifurcation, and to compute boundaries on the eigenvalues of the uncertain system. In this work, we use the SSV to obtain a stability margin, which tells us how much the uncertain parameters can vary before losing closed-loop stability, and allows us to identify the smallest level of uncertainty (and corresponding parameterisation) which destabilises the controller.

The value of developing a rigorous theoretical framework for this analysis is demonstrated by the failure of a standard Monte Carlo simulation campaign to find the worst-case uncertainty combination for our example system. Finally, we discuss the applicability of our results to implementations using DSD reactions. CRN-based representations of feedback systems can be unfeasible when mapped into DNA chemistry, since large species concentrations deplete auxiliary DNA fuel species, and even assuming as in [13] that these are replenished, there are physical limits on the rates and concentrations that are achievable. This is addressed in [14] by scaling the magnitude of the concentrations and the response time of the network to ensure a feasible DNA implementation. We show here that robustness results for our CRN representation also hold when the system is subsequently scaled for implementation in nucleic acid-based chemistry.

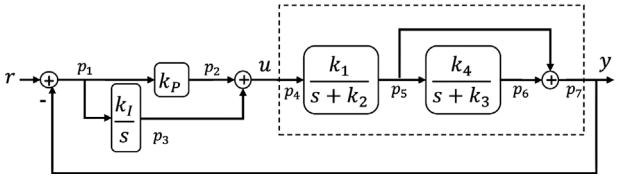

Fig. 1. Closed loop system with second order transfer function.

2. CRN representation of a linear system

A CRN is composed of a set of reactions of chemical species X_j, where the chemical reaction can be approximated by sets of Ordinary Differential Equations (ODE) using mass action kinetics [29], i.e.

$$a_1X_1 + a_2X_2 \xrightarrow{\gamma} bX_3 \Rightarrow \dot{x}_3 = b\gamma x_1^{a_1} x_2^{a_2} \tag{1}$$

The variations in concentration x_j of each species X_j depend on the product of the concentrations, the power of the stoichiometric coefficients a_j and b, and the rate γ.

If we take as an example the second order plant with a zero shown in Fig. 1

$$Y(s) = \frac{k_1}{s+k_2}\left(\frac{s+k_4+k_3}{s+k_3}\right) U(s) \tag{2}$$

the first step is to obtain a chemical reaction network with matching dynamics. For this case, take the set of catalysis and degradation reactions

$$p_4 \xrightarrow{k_1} p_4 + p_5\,,\; p_5 \xrightarrow{k_2} \emptyset \tag{3}$$

$$p_5 \xrightarrow{k_4} p_5 + p_6\,,\; p_6 \xrightarrow{k_3} \emptyset \tag{4}$$

$$p_5 \xrightarrow{\gamma} p_5 + p_7\,,\; p_6 \xrightarrow{\gamma} p_6 + p_7,\; p_7 \xrightarrow{\gamma} \emptyset \tag{5}$$

where $\emptyset$ represents degraded or inactive species. Using (1) and applying the Laplace transform, we can write

$$P_5(s) = k_1(s+k_2)^{-1}P_4(s) \tag{6}$$

$$P_6(s) = k_4(s+k_3)^{-1}P_5(s) \tag{7}$$

Assuming timescale separation (as in the analysis of $\gamma \to \infty$ in [8]), the species p_7 is considered to be at quasi-steady state

$$\dot{p}_7 = \gamma p_5 + \gamma p_6 - \gamma p_7 \approx 0 \Rightarrow p_7 \approx p_5 + p_6 \tag{8}$$

The time scale separation of (5) sets $P_7(s)$ as the sum of the previous transfer functions and

$$P_7(s) = \left(1 + \frac{k_4}{s+k_3}\right) \quad P_5(s) = \frac{(s+k_4+k_3)}{s+k_3}\frac{k_1}{s+k_2}P_4(s) \tag{9}$$

From the CRN we recover the SISO transfer function where the zero depends on the reaction rates k_3 and k_4, and the poles result from the two degradation reaction rates k_2 and k_3.

2.1. Input–output linear system

The concentrations of species in the dynamics of the CRN (3)–(5) are limited to nonnegative values, when in general we need the state to be real with $p_i \in \mathbb{R}$. For a feedback with a Proportional–Integration controller as in Fig. 1, we need to represent negative and positive errors p_1. This limitation is overcome with the *dual rail* representation in [8] and the methodology in [13], which can express any SISO transfer function as a CRN.

In the *dual rail* decomposition [8], each signal is split into two contributions $p_j = x_j^+ - x_j^-$, where x_j^+ and x_j^- are chemical

species concentrations. The CRN for $x_j^{\pm}$ is then used to define an Input–Output (I/O) linear system $G(s)$ such that for Fig. 1 we have

$$\left(y^+ - y^-\right) = G(s)\left(r^+ - r^-\right) \tag{10}$$

For our plant CRN (3)–(5), we define the dual sets of reactions as

$$x_4^{\pm} \xrightarrow{k_1} x_4^{\pm} + x_5^{\pm},\ x_5^{\pm} \xrightarrow{k_2} \emptyset \tag{11}$$

$$x_5^{\pm} \xrightarrow{k_4} x_5^{\pm} + x_6^{\pm},\ x_6^{\pm} \xrightarrow{k_3} \emptyset \tag{12}$$

$$x_5^{\pm} \xrightarrow{\gamma} x_5^{\pm} + x_7^{\pm},\ x_6^{\pm} \xrightarrow{\gamma} x_6^{\pm} + x_7^{\pm},\ x_7^{\pm} \xrightarrow{\gamma} \emptyset \tag{13}$$

$$x_5^{+} + x_5^{-} \xrightarrow{\eta} \emptyset,\ x_6^{+} + x_6^{-} \xrightarrow{\eta} \emptyset,\ x_7^{+} + x_7^{-} \xrightarrow{\eta} \emptyset \tag{14}$$

With the superscript notation $x^{\pm}$, we simultaneously represent reactions for both x^+ and x^- where

$$\left.\begin{array}{l} x^{+} \xrightarrow{k} x^{+} + y^{+} \\ x^{-} \xrightarrow{k} x^{-} + y^{-} \end{array}\right\} \Leftrightarrow x^{\pm} \xrightarrow{k} x^{\pm} + y^{\pm} \tag{15}$$

The parameters γ and η are the rates for the auxiliary reactions of catalysis, degradation, and annihilation as defined in [8].

The remaining linear operations in the feedback loop can be found in literature (see e.g., [8,17,30]). The CRN for the two-sided subtraction in signal $p_1 = r - y = r - p_7$ is

$$r^{\pm} \xrightarrow{\gamma} r^{\pm} + x_1^{\pm}, \qquad x_7^{\pm} \xrightarrow{\gamma} x_7^{\pm} + x_1^{\mp} \tag{16}$$

$$x_1^{\pm} \xrightarrow{\gamma} \emptyset, \qquad x_1^{+} + x_1^{-} \xrightarrow{\eta} \emptyset \tag{17}$$

The CRN for the gain $p_2 = k_P p_1$ is:

$$x_1^{\pm} \xrightarrow{\gamma k_P} x_1^{\pm} + x_2^{\pm},\quad x_2^{\pm} \xrightarrow{\gamma} \emptyset,\quad x_2^{+} + x_2^{-} \xrightarrow{\eta} \emptyset \tag{18}$$

For the integration $\dot{p}_3 = k_I p_1$ we have

$$x_1^{\pm} \xrightarrow{k_I} x_1^{\pm} + x_3^{\pm}, \qquad x_3^{+} + x_3^{-} \xrightarrow{\eta} \emptyset \tag{19}$$

and finally the summation $p_4 = p_2 + p_3$ is set with:

$$x_2^{\pm} \xrightarrow{\gamma} x_2^{\pm} + x_4^{\pm}, \qquad x_3^{\pm} \xrightarrow{\gamma} x_3^{\pm} + x_4^{\pm} \tag{20}$$

$$x_4^{\pm} \xrightarrow{\gamma} \emptyset, \qquad x_4^{+} + x_4^{-} \xrightarrow{\eta} \emptyset \tag{21}$$

Using (1), the complete set of ODEs is

$$\dot{x}_1^{\pm} = -\gamma x_1^{\pm} + \gamma x_7^{\mp} + \gamma r^{\pm} \qquad - \eta x_1^{+} x_1^{-} \tag{22}$$

$$\dot{x}_2^{\pm} = \gamma k_P x_1^{\pm} - \gamma x_2^{\pm} \qquad - \eta x_2^{+} x_2^{-} \tag{23}$$

$$\dot{x}_3^{\pm} = k_I x_1^{\pm} \qquad - \eta x_3^{+} x_3^{-} \tag{24}$$

$$\dot{x}_4^{\pm} = \gamma x_2^{\pm} + \gamma x_3^{\pm} - \gamma x_4^{\pm} \qquad - \eta x_4^{+} x_4^{-} \tag{25}$$

$$\dot{x}_5^{\pm} = k_1 x_4^{\pm} - k_2 x_5^{\pm} \qquad - \eta x_5^{+} x_5^{-} \tag{26}$$

$$\dot{x}_6^{\pm} = k_4 x_5^{\pm} - k_3 x_6^{\pm} \qquad - \eta x_6^{+} x_6^{-} \tag{27}$$

$$\dot{x}_7^{\pm} = \gamma x_5^{\pm} + \gamma x_6^{\pm} - \gamma x_7^{\pm} \qquad - \eta x_7^{+} x_7^{-} \tag{28}$$

Finally, applying the transformations $p_j = x_j^+ - x_j^-$ and $r = r^+ - r^-$, we get the I/O linear dynamics $\dot{p}_j = \dot{x}_j^+ - \dot{x}_j^-$

$$\dot{\mathbf{p}} = A_p \mathbf{p} + B_p r \tag{29}$$

with $\mathbf{p} = \begin{bmatrix} p_1 & \dots & p_7 \end{bmatrix}^T \in \mathbb{R}^{7\times 1}$, $r \in \mathbb{R}$, and

$$A_p = \begin{bmatrix} -\gamma & 0 & 0 & 0 & 0 & 0 & -\gamma \\ \gamma k_P & -\gamma & 0 & 0 & 0 & 0 & 0 \\ k_I & 0 & 0 & 0 & 0 & 0 & 0 \\ 0 & \gamma & \gamma & -\gamma & 0 & 0 & 0 \\ 0 & 0 & 0 & k_1 & -k_2 & 0 & 0 \\ 0 & 0 & 0 & 0 & k_4 & -k_3 & 0 \\ 0 & 0 & 0 & 0 & \gamma & \gamma & -\gamma \end{bmatrix}, \quad B_p = \begin{bmatrix} \gamma \\ 0_{6\times 1} \end{bmatrix}$$

This linear state space represents the I/O linear response from r to the outputs p_j, and it contains additional dynamics besides the controller and the plant, introduced by the CRN representations of the algebraic operations.

However, the approximation to the feedback loop transfer function improves with the assumption of timescale separation of the dynamics for the linear operators, i.e., if the auxiliary reaction rates $\gamma \to \infty$ [8], some of the signals are at quasi-steady state

$$p_1 \approx r - p_7,\ p_2 \approx k_P p_1,\ p_4 \approx p_2 + p_3,\ p_7 \approx p_5 + p_6 \tag{30}$$

and the remaining dynamics correspond to the initial SISO system

$$\dot{p}_3 \approx k_I p_1 \tag{31}$$

$$\dot{p}_5 \approx k_1 p_4 - k_2 p_5 \tag{32}$$

$$\dot{p}_6 \approx k_4 p_5 - k_3 p_6 \tag{33}$$

3. Nonlinear model of the CRN

The linear system in (29) represents only the dynamics between the input signal r and the signals p_j, and the contribution from the nonlinear terms are removed when we compute $\dot{p}_j = \dot{x}_j^+ - \dot{x}_j^-$. Hence, the impact of the bimolecular annihilation reactions in the dynamics is not observable in the I/O linear system.

To analyse the complete dynamics of the concentrations in the CRN, we define instead the input vector $\mathbf{r} = [r^+ r^-]^T$ and the state vector $\mathbf{x} \geq 0$ such that

$$\mathbf{x} = \begin{bmatrix} x_1^+ & \dots & x_N^+ & x_1^- & \dots & x_N^- \end{bmatrix}^T = \begin{bmatrix} \mathbf{x}^+ \\ \mathbf{x}^- \end{bmatrix} \tag{34}$$

We can use the Hadamard element-wise product $\circ$ and a permutation matrix P to express the bimolecular terms, and compact the ODEs into

$$\dot{\mathbf{x}} = A\mathbf{x} + B\mathbf{r} - \eta\,(P\mathbf{x}) \circ \mathbf{x} \tag{35}$$

where $P = \begin{bmatrix} 0 & I \\ I & 0 \end{bmatrix}$.

In its natural coordinates $x_j^{\pm}$ the dynamics result in a positive system [31], and contains nonlinearities. Furthermore, the I/O dynamics assumes that the representation of the signals p_j depends only on x_j^+ or x_j^- at each instant, as a result of very fast annihilation reactions $x_j^+ + x_j^- \xrightarrow{\eta} \emptyset$. However, for a finite reaction rate η, the system can have a positive equilibrium in which both dual species x_j^+ and x_j^- coexist.

The dynamics (31)–(33) also depend on the assumption that $k_j^+ = k_j^-$ and $\gamma_j^+ = \gamma_j^-$. In the nonlinear model, we consider a possible mismatch between the dual rates and consider independent rates for each reaction with

$$x_j^{\pm} \xrightarrow{\gamma_i^{\pm}} x_j^{\pm} + x_i^{\pm},\ x_j^{\pm} \xrightarrow{\gamma_i^{\pm}} \emptyset \tag{36}$$

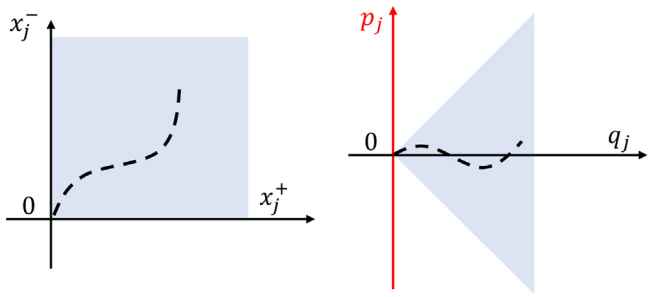

Fig. 2. Transformation from the non-negative natural coordinates $x_j^{\pm}$ on the left, to the new coordinates on the right with $p_j = x_j^+ - x_j^-$ and $q_j = x_j^+ + x_j^-$. The invariant space of the trajectories changes from the positive octant on the left to the cone on the right, where trajectories projected on the ordinate are not restricted to be non-negative $p_j \in \mathbb{R}$, and $q_j \in \mathbb{R}_0^+$.

$$x_j^{\pm} \xrightarrow{k_i^{\pm}} x_j^{\pm} + x_i^{\pm},\ x_j^{\pm} \xrightarrow{k_i^{\pm}} \emptyset \tag{37}$$

We account for the separate rates with the decomposition

$$A = \begin{bmatrix} A_{11}^+ & A_{12}^- \\ A_{12}^+ & A_{11}^- \end{bmatrix}, \quad B = \begin{bmatrix} B_{11}^+ & 0 \\ 0 & B_{11}^- \end{bmatrix}$$

where the submatrices are

$$A_{11}^{\pm} = \begin{bmatrix} -\gamma_3^{\pm} & 0 & 0 & 0 & 0 & 0 & 0 \\ (\gamma_4 k_P)^{\pm} & -\gamma_5^{\pm} & 0 & 0 & 0 & 0 & 0 \\ k_I^{\pm} & 0 & 0 & 0 & 0 & 0 & 0 \\ 0 & \gamma_6^{\pm} & \gamma_7^{\pm} & -\gamma_8^{\pm} & 0 & 0 & 0 \\ 0 & 0 & 0 & k_1^{\pm} & -k_2^{\pm} & 0 & 0 \\ 0 & 0 & 0 & 0 & k_4^{\pm} & -k_3^{\pm} & 0 \\ 0 & 0 & 0 & 0 & \gamma_9^{\pm} & \gamma_{10}^{\pm} & -\gamma_{11}^{\pm} \end{bmatrix}$$

$$A_{12}^{\pm} = \begin{bmatrix} 0_{1\times 6} & \gamma_2^{\pm} \\ 0_{6\times 6} & 0_{6\times 1} \end{bmatrix}, \quad B_{11}^{\pm} = \begin{bmatrix} \gamma_1^{\pm} \\ 0_{6\times 1} \end{bmatrix}$$

3.1. I/O and nonlinear dynamics

The connections between the I/O linear system and the nonlinear dynamics can be seen more clearly with the change of coordinates

$$\begin{bmatrix} \mathbf{p} \\ \mathbf{q} \end{bmatrix} = \begin{bmatrix} W_p \\ W_q \end{bmatrix} \mathbf{x} = \begin{bmatrix} I & -I \\ I & I \end{bmatrix} \mathbf{x} = W\mathbf{x} \tag{38}$$

such that $\mathbf{p} = \mathbf{x}^+ - \mathbf{x}^-$ and $\mathbf{q} = \mathbf{x}^+ + \mathbf{x}^-$, see Fig. 2. This transformation is a global diffeomorphism [32], it is continuously differentiable, its Jacobian is non-singular $\forall \mathbf{x} \in \mathbb{R}^{2N}$, and $\lim_{\|\mathbf{x}\|\to\infty} \| W\mathbf{x} \| = \infty$. The dynamics in these *rotated coordinates* are given by

$$\begin{aligned} \begin{bmatrix} \dot{\mathbf{p}} \\ \dot{\mathbf{q}} \end{bmatrix} &= \frac{1}{2} WAW^T + WB\mathbf{r} + \frac{\eta}{2} \begin{bmatrix} 0 \\ \mathbf{p} \circ \mathbf{p} - \mathbf{q} \circ \mathbf{q} \end{bmatrix} \\ &= \begin{bmatrix} R_{11} & R_{12} \\ R_{21} & R_{22} \end{bmatrix} \begin{bmatrix} \mathbf{p} \\ \mathbf{q} \end{bmatrix} + \begin{bmatrix} W_p \\ W_q \end{bmatrix} B\mathbf{r} + \frac{\eta}{2} \begin{bmatrix} 0 \\ \mathbf{p} \circ \mathbf{p} - \mathbf{q} \circ \mathbf{q} \end{bmatrix} \end{aligned} \tag{39}$$

with

$$\begin{aligned} R_{11} &= 0.5\left(A_{11}^+ + A_{11}^-\right) - 0.5\left(A_{12}^+ + A_{12}^-\right) \\ R_{22} &= 0.5\left(A_{11}^+ + A_{11}^-\right) + 0.5\left(A_{12}^+ + A_{12}^-\right) \\ R_{12} &= 0.5\left(A_{11}^+ - A_{11}^-\right) - 0.5\left(A_{12}^+ - A_{12}^-\right) \\ R_{21} &= 0.5\left(A_{11}^+ - A_{11}^-\right) + 0.5\left(A_{12}^+ - A_{12}^-\right) \end{aligned}$$

The coordinates $\mathbf{p}$ correspond to the states of the I/O dynamics, and the change of coordinates reveals the underlying dynamics $\dot{\mathbf{q}}$, which are not observed in (29).

Let us first consider the nominal case, when $A_{ji}^+ = A_{ji}^- = \bar{A}_{ji}$ and $B_{11}^+ = B_{11}^- = \bar{B}_{11}$. In this case we recover the linear system (29) with $A_p = \frac{1}{2} W_p \bar{A} W_p^T$ and $B_p r = W_p \bar{B}\mathbf{r}$. We have also that $R_{12} = R_{21} = 0$, the I/O dynamics are independent of $\mathbf{q}$, and

$$\dot{\mathbf{q}} = R_{22}\mathbf{q} + \bar{B}_{11}\left(r^+ + r^-\right) + \frac{\eta}{2}\left(\mathbf{p} \circ \mathbf{p} - \mathbf{q} \circ \mathbf{q}\right) \tag{40}$$

The system (40) is non-negative, and it can be shown that it is bounded. The former derives from the system in the natural coordinates which is non-negative: $\mathbf{x} \geq 0$, $\mathbf{r} \geq 0$, $\bar{B} \geq 0$, and $\bar{A}$ is Metzler (off-diagonal elements are nonnegative [31]). Since $\bar{A}$ is Metzler, then $\bar{A}_{11}$, $\bar{A}_{12}$ and $R_{22} = \bar{A}_{11} + \bar{A}_{12}$ are also Metzler. Hence, the system is nonnegative, because for a coordinate at the edge of the octant $\mathbb{R}_0^+$, i.e. $q_j = 0$, it results that $q_j^2 = 0$ and $\dot{q}_j \geq 0$.

To conclude boundedness, consider the Lyapunov function $V = \sum q_j$ $(\forall_{\mathbf{q}>0} : V > 0)$, and the dynamics $\dot{\mathbf{q}} = R_{22}\mathbf{q} - \frac{\eta}{2}\mathbf{q} \circ \mathbf{q} + \mathbf{v}$, $\mathbf{v} \geq 0$. Then

$$\begin{aligned} \dot{V} = \sum \dot{q}_j &= \sum [R_{22}\mathbf{q}]_j - \frac{\eta}{2}\sum q_j^2 + \sum \nu_j \\ &\leq \|R_{22}\mathbf{q}\|_1 - \frac{\eta}{2}\|\mathbf{q}\|_2^2 + \|\mathbf{v}\|_1 \\ &\leq \sqrt{N}\|R_{22}\|_2\|\mathbf{q}\|_2 - \frac{\eta}{2}\|\mathbf{q}\|_2^2 + \|\mathbf{v}\|_1 \\ \dot{V} < 0 \Rightarrow &\left(\frac{\eta}{2}\|\mathbf{q}\|_2 - \sqrt{N}\|R_{22}\|_2\right)\|\mathbf{q}\|_2 > \|\mathbf{v}\|_1 \\ \Rightarrow &\|\mathbf{q}\|_2 > \frac{2}{\eta}\sqrt{N}\|R_{22}\|_2 + \frac{2}{\eta}\frac{\|\mathbf{v}\|_1}{\|\mathbf{q}\|_2} \end{aligned}$$

For the unforced response, it is enough that $\|\mathbf{q}\|_2 > \frac{2}{\eta}\sqrt{N}\|R_{22}\|_2$ to have $\dot{V} < 0$. Even in the presence of a positive input $\mathbf{v}$, there is always a $\mathbf{q}$ large enough so that $\dot{V} < 0$.

This shows that the trajectories $\mathbf{q}$ are bounded for bounded inputs $\mathbf{r}$ and $\mathbf{p}$, and can be limited by increasing the reaction rate η. Hence, with the nominal parameterisation the unobserved nonlinear dynamics do not pose a problem for the CRN representation of the I/O linear dynamics.

However, in general, the parameterisation of the CRN will be affected by variability in the reaction rates, causing mismatches between the submatrices of A and B. The crossed terms become $R_{12} \neq 0$, $R_{21} \neq 0$, and create a feedback loop between the linear and nonlinear dynamics. This motivates the inclusion of the nonlinear dynamics in the stability analysis, since a stable R_{11} does not guarantee the stability of the coupled nonlinear dynamics (39).

3.2. Linearisation and local stability

Both Lyapunov's indirect method and robustness stability analysis provide a local result around the equilibrium of the system. We choose the equilibrium of the unforced non-linear dynamics, for a null input $\mathbf{r}^0 = 0$. We define then $\mathbf{x}^0$ as the solution to

$$A\mathbf{x}^0 - \eta P\mathbf{x}^0 \circ \mathbf{x}^0 = 0 \Leftrightarrow A\mathbf{x}^0 = \eta P\mathbf{x}^0 \circ \mathbf{x}^0 \tag{41}$$

It is noteworthy that, from (41), we have at equilibrium

$$\begin{aligned} &A_{11}^{+}\mathbf{x}^{0+} + A_{12}^{-}\mathbf{x}^{0-} = A_{12}^{+}\mathbf{x}^{0+} + A_{11}^{-}\mathbf{x}^{0-} = \eta\mathbf{x}^{0+} \circ \mathbf{x}^{0-} \\ &\Rightarrow \left(A_{11}^{-} - A_{12}^{-}\right)\mathbf{x}^{0-} = \left(A_{11}^{+} - A_{12}^{+}\right)\mathbf{x}^{0+} \end{aligned} \tag{42}$$

and half of the equilibrium vector is constrained by

$$\mathbf{x}^{0-} = \left(A_{11}^{-} - A_{12}^{-}\right)^{-1}\left(A_{11}^{+} - A_{12}^{+}\right)\mathbf{x}^{0+} \tag{43}$$

For a constant perturbation input $\mathbf{r}_e = \mathbf{r} - \mathbf{r}^0 = \mathbf{r}$, the perturbation trajectories around the equilibrium $\mathbf{x}^0$ are defined as $\mathbf{x}_e = \mathbf{x} - \mathbf{x}^0$, with

$$\begin{aligned} \dot{\mathbf{x}} = &\ \frac{d\mathbf{x}^0}{dt} + \dot{\mathbf{x}}_e \\ \Rightarrow \dot{\mathbf{x}}_e = &\ A\left(\mathbf{x}^0 + \mathbf{x}_e\right) - \eta\left(P\mathbf{x}^0 + P\mathbf{x}_e\right) \circ \left(\mathbf{x}^0 + \mathbf{x}_e\right) + B\mathbf{r}_e \\ = &\ A\mathbf{x}^0 - \eta P\mathbf{x}^0 \circ \mathbf{x}^0 + A\mathbf{x}_e + B\mathbf{r}_e \\ &-\eta\left(P\mathbf{x}^0 \circ \mathbf{x}_e + P\mathbf{x}_e \circ \mathbf{x}^0 + P\mathbf{x}_e \circ \mathbf{x}_e\right) \\ = &\ A\mathbf{x}_e - \eta\left(P\mathbf{x}^0 \circ \mathbf{x}_e + P\mathbf{x}_e \circ \mathbf{x}^0\right) + B\mathbf{r}_e - \eta P\mathbf{x}_e \circ \mathbf{x}_e \\ = &\ \left(A + \eta J\left\{\mathbf{x}^0\right\}\right)\mathbf{x}_e + B\mathbf{r}_e - \eta P\mathbf{x}_e \circ \mathbf{x}_e \end{aligned} \tag{44}$$

where

$$J\left\{\mathbf{x}^0\right\} = -\mathrm{diag}\left\{P\mathbf{x}^0\right\} - \mathrm{diag}\left\{\mathbf{x}^0\right\}P \tag{45}$$

$$= -\begin{bmatrix} \mathrm{diag}\left\{\mathbf{x}^{0-}\right\} & \mathrm{diag}\left\{\mathbf{x}^{0+}\right\} \\ \mathrm{diag}\left\{\mathbf{x}^{0-}\right\} & \mathrm{diag}\left\{\mathbf{x}^{0+}\right\} \end{bmatrix} \tag{46}$$

Linearising the perturbation model around its equilibrium at the origin $\mathbf{x}_e^0 = 0$ we then have

$$\dot{\mathbf{s}} = \left(A + \eta J\left\{\mathbf{x}^0\right\}\right)\mathbf{s} + B\mathbf{r}_e \tag{47}$$

Even if A is not Hurwitz, the linearisation can still be stable if $\mathbf{x}^0 > 0$.

The linearisation relies on the solution to the equilibrium condition (41) subject to the constraint (43), which is not trivial to solve. For the robust stability analysis we need to compute at least the equilibrium for the nominal parameterisation $\bar{\mathbf{x}}^0$. We have seen that for that case, we only need to ensure that by design the nominal I/O dynamics are stable, to have a stable nonlinear system. We can then find $\bar{\mathbf{x}}^0$ by integrating the nominal dynamics with $\mathbf{r} = 0$ and $\mathbf{x}(0) > 0$. The constraint (43) is respected with $\bar{\mathbf{x}}^{0+} = \bar{\mathbf{x}}^{0-}$.

Since we wish to verify the robustness results by checking the local stability with Lyapunov's indirect method, we may need to linearise the dynamics around unstable equilibria, which cannot be found by integrating the dynamics (35). We are able to circumvent this difficulty by defining new dynamics based on the rotated coordinates, where the dynamics for $\dot{\mathbf{p}}$ are replaced by their steady state solution as a function of $\mathbf{q}$ with $\mathbf{p}^0 = -R_{11}^{-1}R_{12}\mathbf{q}^0$. We then obtain the reduced model

$$\begin{aligned} \dot{\mathbf{c}} = &\ \left(R_{22} - R_{21}R_{11}^{-1}R_{12}\right)\mathbf{c} \\ &+\frac{\eta}{2}\left(R_{11}^{-1}R_{12}\mathbf{c}\right) \circ \left(R_{11}^{-1}R_{12}\mathbf{c}\right) - \frac{\eta}{2}\mathbf{c} \circ \mathbf{c} \end{aligned} \tag{48}$$

which can be integrated to find the equilibrium $\mathbf{c}^0$, with $\mathbf{c}(0) = 2\bar{\mathbf{x}}^{0+}$. These constrained dynamics share the same equilibrium as the rotated dynamics, but the feedback interconnection with the I/O dynamics is replaced with a static matrix. The rotated equilibrium is then given by $\mathbf{q}^0 = \mathbf{c}^0$ and $\mathbf{p}^0 = -R_{11}^{-1}R_{12}\mathbf{c}^0$. The equilibrium in natural coordinates is finally recovered with $\mathbf{x}^{0\pm} = \mathbf{q}^0 \pm \mathbf{p}^0$.

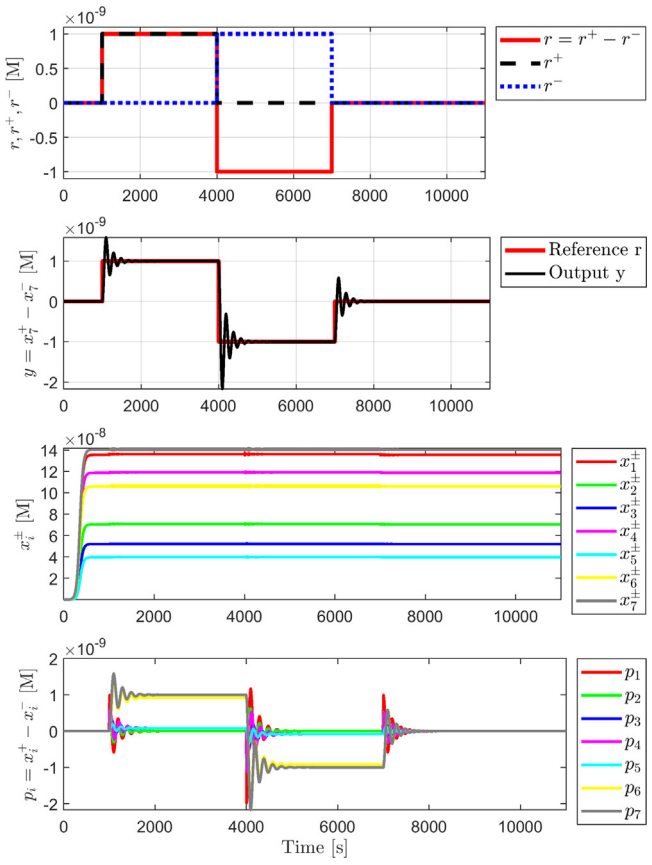

Fig. 3. Nominal time response of the reference input r and the tracking output y. The reference signal $r = r^+ - r^-$ is such that only one of the $r^\pm$ components exist at each given time at steady state, resulting in the ideal sequence of reference steps. The concentrations $x_i^\pm$ converge to a positive equilibrium even if $r^\pm = 0$, and the differences between the dual concentrations represent the state of the I/O linear dynamics p_i.

3.3. Uncertainty and equilibrium model

The implementation of the CRNs is limited by the predictability of the affinities in the biomolecular network [33]. This leads to variability on the reaction rates and uncertainty in the implemented network. Moreover, in the case of the nonlinear system (35), the equilibrium moves depending on the parameterisation [27]. Hence, the linearisation depends on the uncertainty both through A and $\mathbf{x}^0$.

Since we do not have an analytical solution for the equilibrium we cannot express explicitly this dependency in the linearised system. Instead, we model the equilibrium variation as an approximate function of the uncertain state matrix and the nominal conditions.

Let us define the nominal matrix $\bar{A}$, where there is no uncertainty and $A_{11}^{+} = A_{11}^{-} = \bar{A}_{11}$, $A_{12}^{+} = A_{12}^{-} = \bar{A}_{12}$, and $B_{11}^{+} = B_{11}^{-} = \bar{B}_{11}$. The nominal equilibrium $\bar{\mathbf{x}}^0$ is then defined such that

$$\bar{A}\bar{\mathbf{x}}^0 - \eta P\bar{\mathbf{x}}^0 \circ \bar{\mathbf{x}}^0 = 0 \tag{49}$$

Lemma

If the variation in the equilibrium $\mathbf{e} = \mathbf{x}^0 - \bar{\mathbf{x}}^0$ *is small with* $|\bar{x}_j^0| > |e_j|$, *then the equilibrium* $\mathbf{x}^0$ *can be approximated by*

$$\hat{\mathbf{x}}^0 := -\left(A + \eta J\left\{\bar{\mathbf{x}}^0\right\}\right)^{-1}\bar{A}\bar{\mathbf{x}}^0 \tag{50}$$

Proof

From the equilibrium condition

$$0 = A\mathbf{x}^0 - \eta P\left(\bar{\mathbf{x}}^0 + \mathbf{e}\right) \circ \left(\bar{\mathbf{x}}^0 + \mathbf{e}\right) \tag{51}$$

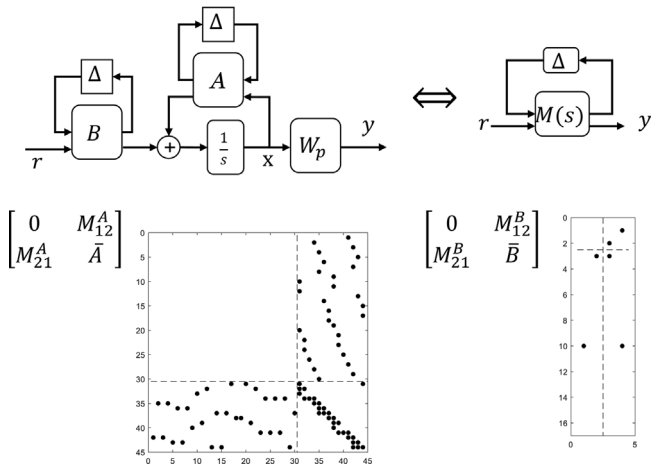

Fig. 4. The uncertainties in the matrices of the CRN dynamics A and B are aggregated into the SSV M-Δ structure. Below are the sparsities of the M structure of matrices A (with 30 uncertainties) and B (with 2).

We extend the nonlinear product into

$$\begin{aligned} 0 = \quad & A\mathbf{x}^0 - \eta\left(P\bar{\mathbf{x}}^0 \circ \mathbf{e} + \bar{\mathbf{x}}^0 \circ P\mathbf{e}\right) - \eta P\bar{\mathbf{x}}^0 \circ \bar{\mathbf{x}}^0 - \eta P\mathbf{e} \circ \mathbf{e} \Rightarrow \\ 0 = \quad & A\mathbf{x}^0 + \eta J\left\{\bar{\mathbf{x}}^0\right\}\mathbf{e} - \eta P\bar{\mathbf{x}}^0 \circ \bar{\mathbf{x}}^0 - \eta P\mathbf{e} \circ \mathbf{e} \end{aligned} \tag{52}$$

With small relative variations in the equilibrium $|\bar{x}_j^0| > |e_j|$, then $|P\bar{\mathbf{x}}^0 \circ \bar{\mathbf{x}}^0| \gg |P\mathbf{e} \circ \mathbf{e}|$ and

$$0 \approx A\mathbf{x}^0 + \eta J\left\{\bar{\mathbf{x}}^0\right\}\mathbf{e} - \eta P\bar{\mathbf{x}}^0 \circ \bar{\mathbf{x}}^0 \tag{53}$$

Replacing $\mathbf{e} = \mathbf{x}^0 - \bar{\mathbf{x}}^0$ we get

$$0 \approx A\mathbf{x}^0 + \eta J\left\{\bar{\mathbf{x}}^0\right\}\mathbf{x}^0 - \eta J\left\{\bar{\mathbf{x}}^0\right\}\bar{\mathbf{x}}^0 - \eta P\bar{\mathbf{x}}^0 \circ \bar{\mathbf{x}}^0 \tag{54}$$

$$\Rightarrow \left(A + \eta J\left\{\bar{\mathbf{x}}^0\right\}\right)\mathbf{x}^0 \approx \eta J\left\{\bar{\mathbf{x}}^0\right\}\bar{\mathbf{x}}^0 + \eta P\bar{\mathbf{x}}^0 \circ \bar{\mathbf{x}}^0 \tag{55}$$

Furthermore,

$$\eta J\left\{\bar{\mathbf{x}}^0\right\}\bar{\mathbf{x}}^0 + \eta P\bar{\mathbf{x}}^0 \circ \bar{\mathbf{x}}^0 = -2\eta P\bar{\mathbf{x}}^0 \circ \bar{\mathbf{x}}^0 + \eta P\bar{\mathbf{x}}^0 \circ \bar{\mathbf{x}}^0 \tag{56}$$

$$= -\eta P\bar{\mathbf{x}}^0 \circ \bar{\mathbf{x}}^0 = -\bar{A}\bar{\mathbf{x}}^0 \tag{57}$$

Since $A + \eta J\left\{\bar{\mathbf{x}}^0\right\}$ is always invertible, we arrive at the defined estimator $\hat{\mathbf{x}}^0$. □

The analysis including the moving equilibrium (ME) uses the linearised dynamics with

$$\dot{\mathbf{s}} = \left(A + \eta J\left\{\hat{\mathbf{x}}^0\right\}\right)\mathbf{s} + B\mathbf{r}_e \tag{58}$$

The definition in (50) respects the constraint

$$\hat{\mathbf{x}}^{0-} = \left(A_{11}^- - A_{12}^-\right)^{-1}\left(A_{11}^+ - A_{12}^+\right)\hat{\mathbf{x}}^{0+} \tag{59}$$

avoiding the introduction of conservatism with respect to (43). However, the use of this model is limited by the assumption of small variations in the equilibrium. The fitting error should be checked since for higher uncertainty intervals, the assumption may be invalid.

4. Robust stability analysis

For the simulation and analysis, the nominal parameterisation is $k_1 = k_2 = 0.01\,\mathrm{s}^{-1}$, $k_3 = 0.0163\,\mathrm{s}^{-1}$, $k_4 = 0.185\,\mathrm{s}^{-1}$ for the plant, and $k_I = 0.01\,\mathrm{s}^{-1}$, $k_P = 0.53$ for the controller. The auxiliary rates were set at $\gamma = 10 \times k_4 = 1.85\,\mathrm{s}^{-1}$, faster than the remaining dynamics, and the annihilation rate at $\eta = 5 \times 10^5\,(\mathrm{Ms})^{-1}$, as in [8]. The time response of the nominal system in Fig. 3 shows the I/O system signal y tracking the reference input r. A positive initial condition $x_j(0) > 0$ causes the concentrations to converge and remain in the nominal operating equilibrium even if $r^{\pm} = 0$.

4.1. μ-analysis

The structured singular value (SSV) framework, or μ-analysis, is an established validation method for uncertain LTI systems representing the infinite family of $G(s, \Delta)$ [25]. The structure of Δ is typically a block diagonal of real and normalised uncertainties such that $|\Delta| \leq 1$, and μ is defined as the inverse of the minimum possible value of Δ that destabilises the system [24,26]. The value of μ is approximated by upper and lower bounds, and if the upper-bound of $1/\mu < 1$ for all frequencies, then $G(s, \Delta)$ is robust to all possible parameterisations.

We used Matlab™ and the Robust Control Toolbox™ [34], to build and manipulate the uncertain systems, and the μ bounds are computed with the function `robstab` and its default options. To build the uncertain systems, each reaction rate is set as an `ureal` object with a multiplicative real variation, e.g., $\delta_1 \in \mathbb{R} : \gamma_1^+ = \bar{\gamma}_1^+\left(1 + \delta_{\gamma_1^+}\right)$. This results in a total of 32 uncertain rates, which are set as the elements of the uncertain matrices A and B used to build the uncertain state space (`uss` object), Fig. 4.

The robustness analysis is carried for $|\Delta| \leq 7\%$, with:

- a) a linearisation around a *fixed equilibrium* (FE), using the nominal equilibrium $\left(A + \eta J\left\{\bar{\mathbf{x}}^0\right\}\right)$;
- b) a linearisation around the *moving equilibrium* (ME) using the estimation $\left(A + \eta J\left\{\hat{\mathbf{x}}^0\right\}\right)$.

The linearisation around a FE results in a Δ_{FE} matrix 32×32, with diagonal real uncertainties, where each uncertainty occurs only once. In the linearisation with ME, the moving equilibrium $\hat{\mathbf{x}}^0$ is computed with (50) and used to build $J\left\{\hat{\mathbf{x}}^0\right\}$. The matrix Δ_{ME} also results real and diagonal, but becomes 452×452, where each uncertainty occurs 15 times (except for $\gamma_1^{\pm}$ which are not used in $\hat{\mathbf{x}}^0$, and therefore occur only once). The structures can be represented by:

$$\begin{aligned} \Delta_{FE} &= \left\{\mathrm{diag}\left[\delta_1, \delta_2, \ldots, \delta_{32}\right] : \delta_i \in \mathbb{R}\right\} \\ \Delta_{ME} &= \left\{\mathrm{diag}\left[\delta_1, \delta_2, \delta_3 I_{15}, \ldots, \delta_{32} I_{15}\right] : \delta_i \in \mathbb{R}\right\} \end{aligned}$$

where I_{15} is the 15×15 identity matrix. The structures of matrix $M(s)$ for the LFTs in both cases are detailed in Fig. 5. They show clearly the increase in size but also complexity of the LFT in the ME case, where D_{11}^{ME} is composed of diagonals coupling all uncertainties.

Fig. 6 shows the normalised distributions of the equilibrium for 10,000 sampled systems and confirms a movement of 20% to 50% due to uncertainty. For each sample, the true equilibrium $\mathbf{x}^0$ is compared with its estimation $\hat{\mathbf{x}}^0$ in Fig. 7, showing a small relative difference to the nominal equilibrium.

The bounds for μ are shown in Fig. 8 and indicate that the linearisation around the fixed nominal equilibrium (FE) is marginally stable, with stability assured only up to $|\Delta| = 6.763\%$. It identified a worst-case uncertainty combination at $\left|\Delta_{FE}\right| = 9.037\%$ which results in a pair of imaginary poles $-9.7 \times 10^{-14} \pm 0.034064i$. The bounds are lower for the μ-analysis with the moving equilibrium model (58), and the linearisation is robust up to $|\Delta| = 7.016\%$. The minimum destabilising $\left|\Delta_{ME}\right| = 9.720\%$ is also higher than with a FE, and results in the pair of poles $7.102 \times 10^{-15} \pm 0.038551i$.

Thus, using the moving equilibrium model includes more effects of the uncertainty in the linearisation, hence reducing conservatism in the analysis.

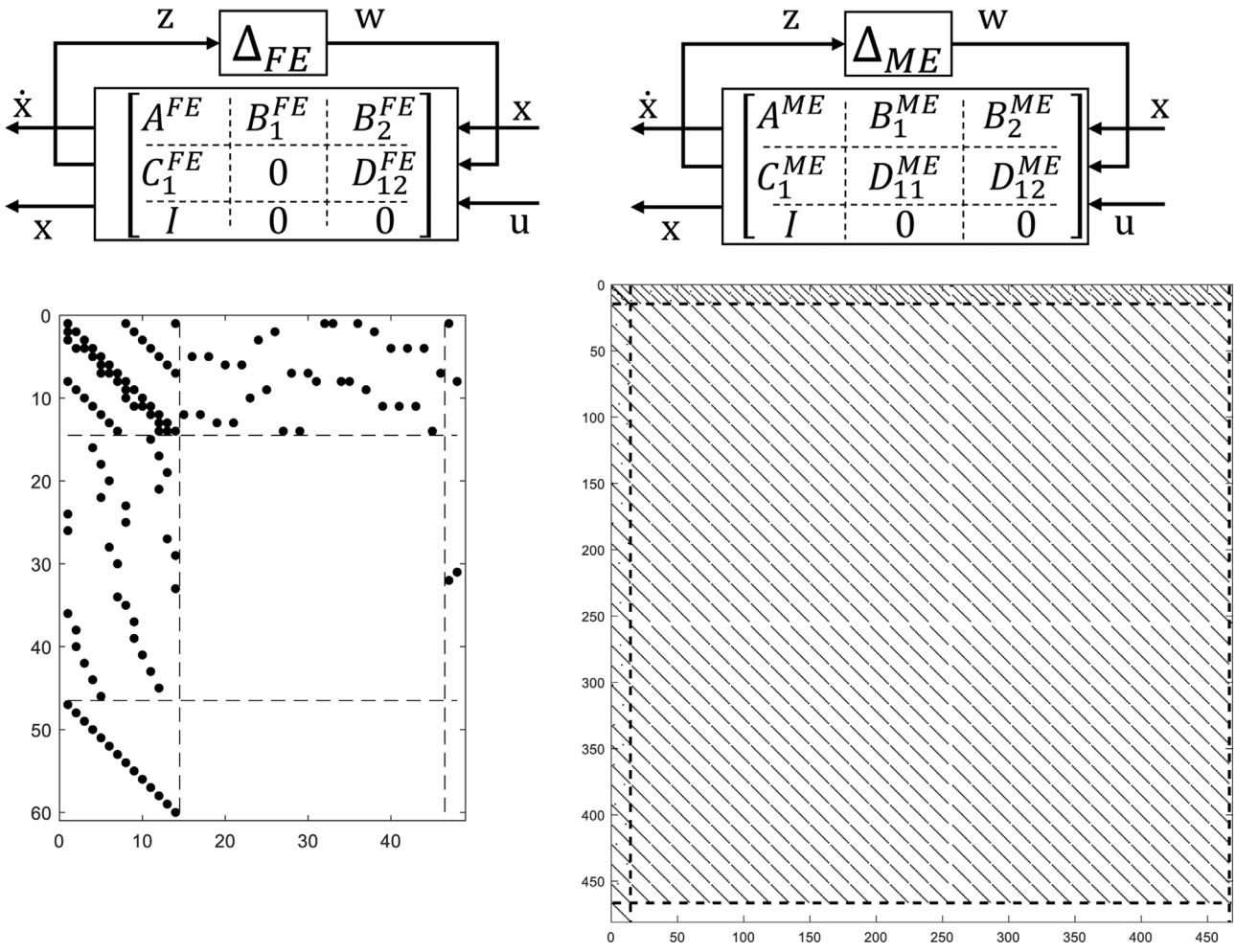

Fig. 5. Structure of the matrix M in the M-Δ decomposition for both of the analysed cases FE (left) and ME (right). The LFT for ME is much larger, and the uncertainties are coupled through D_{11}^{ME}.

4.2. Verification with the nonlinear system

We carried out a Monte Carlo campaign for a variability in the reaction rates of $|\Delta_{MC}| = 10\%$, where all elements of A and B were scattered 10,000 times. For each parameter vector, the equilibrium is solved using (48) and the local stability is checked using the linearised system (47). All the sampled parameterisations in this Monte Carlo campaign resulted in stable closed-loop systems, with the eigenvalues closest to the imaginary axis at $-0.00237686 \pm 0.0325045i$.

We also performed an iterative search for a destabilising parameterisation, where for each level of $|\Delta|$, 2^{12} out of 2^{32} possible vertices of the parameter space are randomly selected and evaluated for stability. The magnitude of the uncertainty $|\Delta|$ is updated heuristically, and in total, 34,144 cases were evaluated. The history of tested magnitudes $\left|\Delta\right|$ and the number of simulations for each value of $\left|\Delta\right|$ is presented in Fig. 9. The minimum destabilising amplitude was found at $\left|\Delta_{IT}\right| = 11.118\%$.

Thus, both Monte Carlo simulation and a brute-force vertices search suggest the system is robust for uncertainty levels up to 10%. This contradicts the destabilising levels of uncertainty identified with the μ bounds, which are now verified directly with the nonlinear system. For each set of destabilising parameters, the dynamics are linearised around their true equilibrium, and the respective poles are compared in Table 1.

Table 1
Verification of destabilising parameterisations with the nonlinear system: eigenvalues of the linearisation around the true equilibrium for each identified parameterisation.

RS with $\bar{\mathbf{x}}^0(\mathbf{k})$ $\lvert\Delta_{FE}\rvert = 9.037\%$	RS with $\hat{\mathbf{x}}^0(\mathbf{k})$ $\lvert\Delta_{ME}\rvert = 9.720\%$	Vertice search $\left\lvert\Delta_{IT}\right\rvert = 11.118\%$
$\mathbf{-0.001073 \pm 0.03361i}$	$\mathbf{+1.916 \times 10^{-6} \pm 0.03855i}$	$\mathbf{+3.399 \times 10^{-5} \pm 0.03242i}$
$-2.296 \pm 0.2353i$	$-2.224 \pm 0.2435i$	$-2.261 \pm 0.2204i$
-2.268	-2.196	-2.265
$-1.92 \pm 0.3411i$	$-1.795 \pm 0.3598i$	$-1.866 \pm 0.3149i$
$-1.718 \pm 0.2867i$	$-1.652 \pm 0.2821i$	$-1.66 \pm 0.253i$
-1.44	-1.344	-1.4
-0.1403	-0.1486	-0.1311
-0.07358	-0.08013	-0.07016
-0.03283	-0.03356	-0.02978
-0.02103	-0.02551	-0.02375

The unstable parameterisation found with the FE actually results in a stable system. Instead of poles on the imaginary axis, the critical poles around true equilibrium are stable at $-0.001073 \pm 0.03361i$. On the other hand, the unstable linearisation with the ME does correspond to an unstable nonlinear system with poles close to the imaginary axis at $+1.916 \times 10^{-6} \pm 0.03855i$, again confirming that use of the ME more accurately captures the impact of the

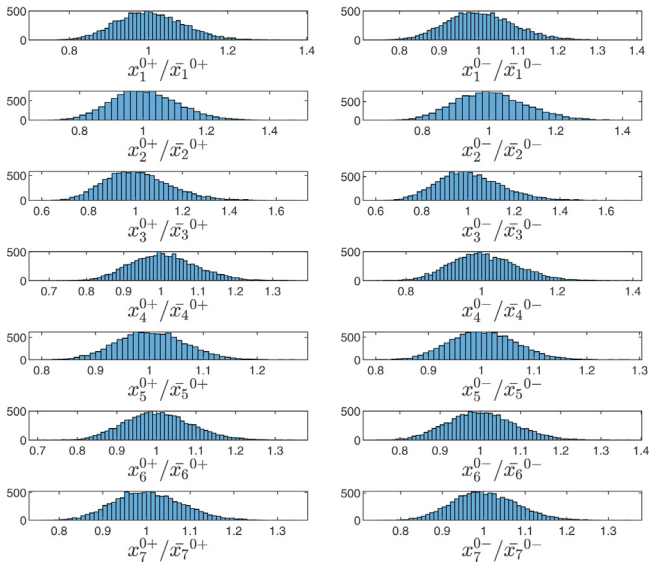

Fig. 6. Distribution of the elements of the moving equilibrium x_j^0, for the 10,000 uncertainty samples. The deviations with respect to nominal equilibrium values $\bar{x}_j^0$ are ±20% to ±50%.

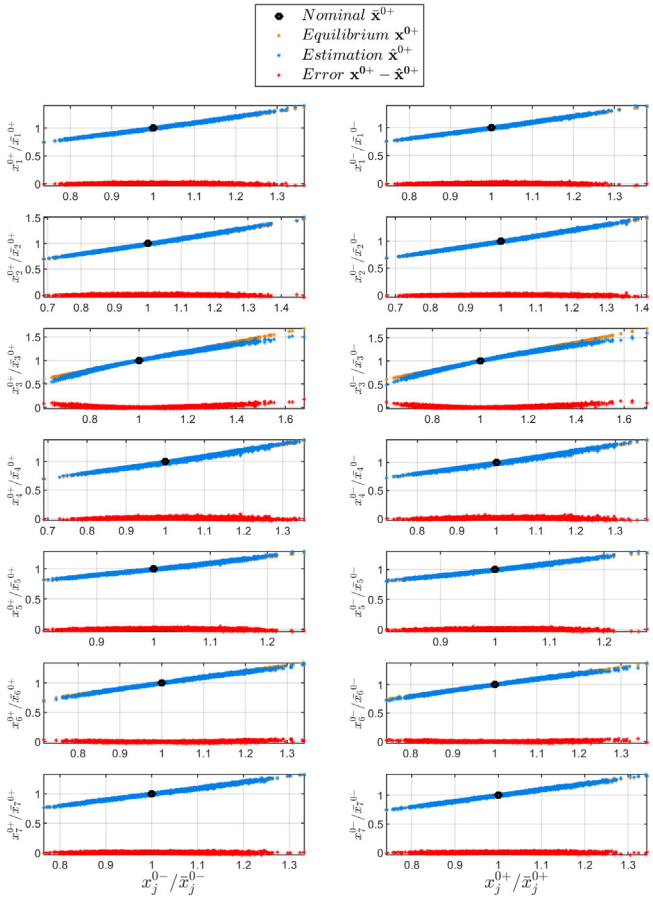

Fig. 7. Comparison between the approximation and the numerically determined element j of the equilibrium, for each of 10,000 samples. In yellow are the true equilibria $\mathbf{x}^0$, in blue are the approximated equilibria $\hat{\mathbf{x}}^0$, and in red are the approximation errors. The axes are normalised by the nominal equilibrium values, hence the nominal value of each element $\bar{x}_j^0$ is mapped into coordinates (1, 1).

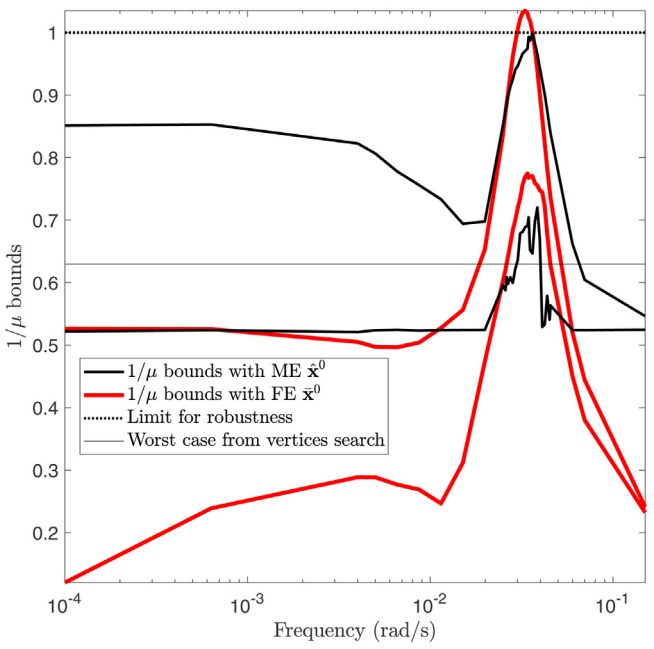

Fig. 8. Comparison of μ bounds with fixed (FE) and moving equilibria (ME). The bounds are lower for the ME case, which includes the equilibrium variation in the linearisation.

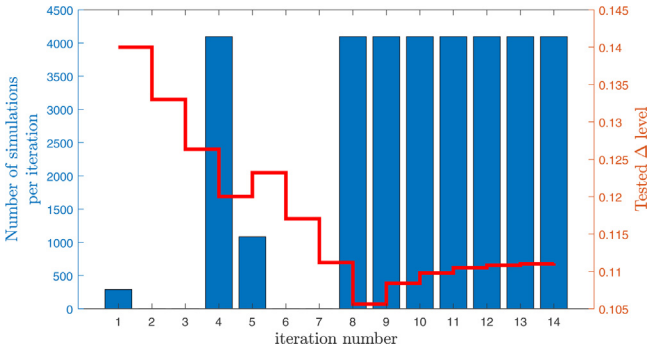

Fig. 9. History of simulations per iteration in the search of a minimum destabilising bound, and the history of tested levels of Δ.

uncertainties on the system, including loss of stability. Furthermore, the unstable parameterisation identified with the ME model is inside the parameter space covered in the Monte Carlo campaign, showing that analysis based on sampling methods can be unreliable since there is no guarantee of complete coverage of the uncertainty space.

5. Robustness levels are independent of scaling for feasibility of DNA implementation

So far we have focused on the analysis of the CRN representation of the biomolecular control system, without addressing the implementation using DSD reactions, which has its own challenges. In particular, there is a physical limit for the bimolecular rate η, which is usually set close to the maximum hybridisation rate around $10^6\,(\text{Ms})^{-1}$ [33,35]. This, together with limits in concentrations, can impose constraints incompatible with the parameterisation of the CRN.

5.1. Scaling for feasibility with DNA chemistry

For the cases where the parameterisation of the CRN is not feasible for an implementation with DSD reactions, the procedure in [14] scales down the parameters to obtain feasible reaction rates and an

accurate representation of the CRN. It exploits the fact pointed out in [14] that, if $\mathbf{z}(t)$ is a solution to the ODEs of the CRN, then given two scalars $a, b > 0$, the function $b\mathbf{z}(\frac{1}{a}t)$ is also a solution to the ODEs, where the unimolecular rates γ_i are scaled by a^{-1}, the bimolecular rate η by $a^{-1}b^{-1}$, and the concentrations get scaled by b.

Let us define a basis dynamics

$$\dot{\mathbf{z}} = \frac{d\mathbf{z}}{dt} = A_z\mathbf{z} + B_z\mathbf{r} - \eta_z P\mathbf{z}\circ\mathbf{z} \tag{60}$$

with a bimolecular reaction η_z, and the unimolecular reaction rates in the network are the elements of A_z. Define $\mathbf{z}^0$ as the equilibrium solution of $A_z\mathbf{z}^0 = \eta_z P\mathbf{z}^0\circ\mathbf{z}^0$, where $\mathbf{z}^0$ depends only on ${\eta_z}^{-1}A_z$. Now define the scaled version of the system with $\mathbf{x} = b\mathbf{z}(\tau)$ where $\tau = \frac{1}{a}t$. The scaled dynamics result

$$\dot{\mathbf{x}} = \frac{d\mathbf{x}}{dt} = b\frac{d\mathbf{z}}{d\tau}\frac{d\tau}{dt} = a^{-1}b\dot{\mathbf{z}} \tag{61}$$

With $A = a^{-1}A_z$, $B = a^{-1}B_z$, $\eta = \frac{1}{ab}\eta_z$, this results in

$$a^{-1}b\dot{\mathbf{z}} = a^{-1}bA_z\mathbf{z} + a^{-1}bB_z\mathbf{r} - a^{-1}b\eta_z P\mathbf{z}\circ\mathbf{z} \tag{62}$$

$$\Rightarrow \dot{\mathbf{x}} = a^{-1}A_z b\mathbf{z} + a^{-1}B_z b\mathbf{r} - a^{-1}b\eta_z P\mathbf{z}\circ\mathbf{z} \tag{63}$$

$$= a^{-1}A_z\mathbf{x} + a^{-1}B_z b\mathbf{r} - a^{-1}b^{-1}\eta_z P\mathbf{x}\circ\mathbf{x} \tag{64}$$

$$= A\mathbf{x} + Bb\mathbf{r} - \eta P\mathbf{x}\circ\mathbf{x} \tag{65}$$

For the scaled solution, we must also scale the input with $b\mathbf{r}$. If the unimolecular rates are not scaled ($a = 1$) then b only scales the concentrations of the system, without changing the poles and response time of the system.

Fig. 10 compares the time response of the system for scalings that result in very large concentrations ($a = 0.01$, $\eta = 0.5$), and in very low concentrations ($a = 100$, $\eta = 5\times10^8$). If we reverse the scaling in the axes of time and concentrations, the time histories are identical.

Scaling the dynamics $A = a^{-1}A_z$, the equilibrium solutions hold if $\mathbf{x}^0 = b\mathbf{z}^0$:

$$A_z\mathbf{z}^0 = \eta_z P\mathbf{z}^0\circ\mathbf{z}^0 \Rightarrow ab^{-1}A\mathbf{x}^0 = b^{-2}\eta_z P\mathbf{x}^0\circ\mathbf{x}^0 \tag{66}$$

$$\Rightarrow A\mathbf{x}^0 = \frac{\eta_z}{ab}P\mathbf{x}^0\circ\mathbf{x}^0 = \eta P\mathbf{x}^0\circ\mathbf{x}^0. \tag{67}$$

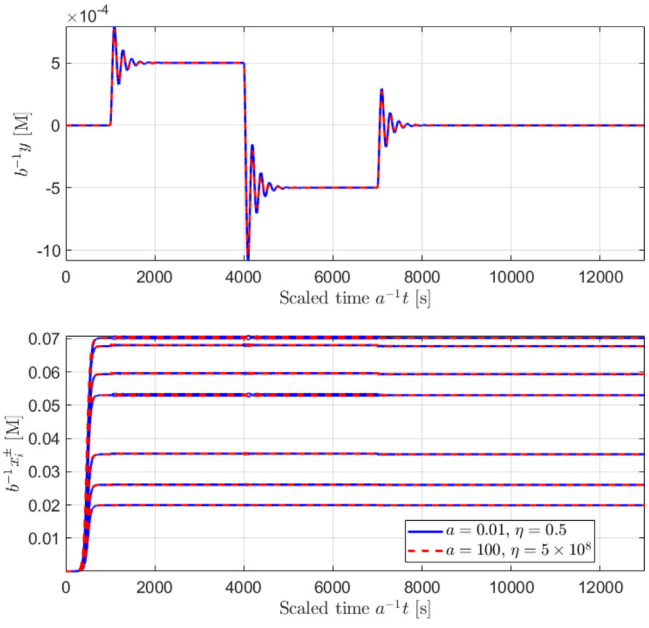

Fig. 10. Time histories of the scaled output and concentrations for two examples with opposite values of $b = (a\eta)^{-1} = 200$ and $b = (a\eta)^{-1} = 2\times10^{-11}$. The time is scaled by a^{-1} to adjust for the change in dynamics speed. The concentrations are scaled by b^{-1}, and the reference input is scaled in both cases $b^{-1}r = 5\times10^{-4}$ [M].

The dynamics of the perturbation $\mathbf{z}_e = \mathbf{z} - \mathbf{z}^0$ are given by

$$\dot{\mathbf{z}}_e = \left(A_z + \eta_z J\left\{\mathbf{z}^0\right\}\right)\mathbf{z}_e + B\mathbf{r}_e - \eta_z P\mathbf{z}_e\circ\mathbf{z}_e \tag{68}$$

and its linearisation around the equilibrium $\mathbf{z}^0$ is given by

$$\dot{\mathbf{h}} = \left(A_z - \eta_z\mathrm{diag}\left\{P\mathbf{z}^0\right\} - \eta_z\mathrm{diag}\left\{\mathbf{z}^0\right\}P\right)\mathbf{h} + B_z\mathbf{r}_e \tag{69}$$

$$= \left(A_z + \eta_z J\left\{\mathbf{z}^0\right\}\right)\mathbf{h} + B_z\mathbf{r}_e \tag{70}$$

Defining the scaled perturbation $\mathbf{x}_e = b\left(\mathbf{z} - \mathbf{z}^0\right)$ and linearisation $\mathbf{s} = b\mathbf{h}$, then $\dot{\mathbf{s}} = a^{-1}b\dot{\mathbf{h}}$ with

$$a^{-1}b\dot{\mathbf{h}} = a^{-1}b\left(A_z + \eta_z J\left\{\mathbf{z}^0\right\}\right)\mathbf{h} + a^{-1}bB_z\mathbf{r}_e \tag{71}$$

$$\Rightarrow \dot{\mathbf{s}} = a^{-1}\left(A_z + \eta_z J\left\{\mathbf{z}^0\right\}\right)\mathbf{s} + a^{-1}B_z b\mathbf{r}_e \tag{72}$$

$$= a^{-1}\left(aA + \eta_z J\left\{b^{-1}\mathbf{x}^0\right\}\right)\mathbf{s} + Bb\mathbf{r}_e \tag{73}$$

$$= \left(A + \eta J\left\{\mathbf{x}^0\right\}\right)\mathbf{s} + Bb\mathbf{r}_e \tag{74}$$

While the concentrations of the input are scaled by b, the state matrix is scaled directly in the new matrix A and the new equilibrium $\mathbf{x}^0$. For a fixed b, the poles of the linearisation are scaled by a^{-1} changing the timescale of the system dynamics without scaling the concentrations.

5.2. Robustness of scaled parameterisations

If the nonlinear dynamics (60) is locally robustly stable, is the scaled system (65) also robustly stable? We now show how the scaling procedure does not affect the robust stability, and the robustness of the original CRN is preserved in the scaled CRNs.

In terms of stability, if $\left(A_z + \eta_z J\left\{\mathbf{z}^0\right\}\right)$ is Hurwitz, then the scaled matrix $a^{-1}\left(A_z + \eta_z J\left\{\mathbf{z}^0\right\}\right) = \left(A + \eta J\left\{\mathbf{x}^0\right\}\right)$ is also Hurwitz. This means that if the system is locally stable at $\mathbf{z}^0$ then the scaled system is locally stable at $\mathbf{x}^0$. If $\dot{\mathbf{h}}$ is stable for any $|\Delta| < 1$, then $a^{-1}\left(A_z + \eta_z J\left\{\mathbf{z}^0\right\}\right)$ is Hurwitz for any $|\Delta| < 1$. Hence, if $\dot{\mathbf{h}}$ is robust then $\dot{\mathbf{s}}$ is also robust, independent of the scaling used.

Consider $\bar{A}_z$ as the nominal dynamics of the original system, with the nominal equilibrium solution $\bar{\mathbf{z}}^0$. The same properties hold by scaling the estimator of the moving equilibrium with $\hat{\mathbf{x}}^0 = b\hat{\mathbf{z}}^0$:

$$b\hat{\mathbf{z}}^0 = -b\left(A_z + \eta_z J\left\{\bar{\mathbf{z}}^0\right\}\right)^{-1}\bar{A}_z\bar{\mathbf{z}}^0 \tag{75}$$

$$= -\left(A_z + \eta_z J\left\{\bar{\mathbf{z}}^0\right\}\right)^{-1}\bar{A}_z\bar{\mathbf{x}}^0 \tag{76}$$

$$= -\left(A + \eta J\left\{\bar{\mathbf{x}}^0\right\}\right)^{-1}\bar{A}\bar{\mathbf{x}}^0 = \hat{\mathbf{x}}^0 \tag{77}$$

Hence, the results still apply if we replace the equilibria $\mathbf{x}^0$ and $\mathbf{z}^0$ with their estimations $\hat{\mathbf{x}}^0$ and $\hat{\mathbf{z}}^0$.

In Fig. 11, the robust stability was investigated for the same system, but scaling the dynamics with a and the equilibrium with η. The bounds for both ME and FE are in general very similar, apart from the shift in frequency due to a. With ME, for very small $b = 1/(a\eta) \leq 5\times10^{-8}$, the upper bound does change. However, this may be due to numerical issues in the computation of $J\{\bar{\mathbf{x}}^0\}$, with the very small values of $\bar{\mathbf{x}}^0$ in Fig. 12. Any numerical discrepancies are then amplified by a large η and the computation of the inversion $\left(A + \eta J\left\{\bar{\mathbf{x}}^0\right\}\right)^{-1}$ in the estimator $\hat{\mathbf{x}}^0$.

Nevertheless, the destabilising $|\Delta_{IT}|$ in Fig. 13, found by testing the vertices of the parameter space, are comparable for all combinations of the scaling. This suggests there are no changes to the upper bounds, including the numerically difficult ones.

This invariance to scaling means that the robustness results with $\dot{\mathbf{z}}$ are applicable for any scaled system $\dot{\mathbf{x}}$, and decouples the design

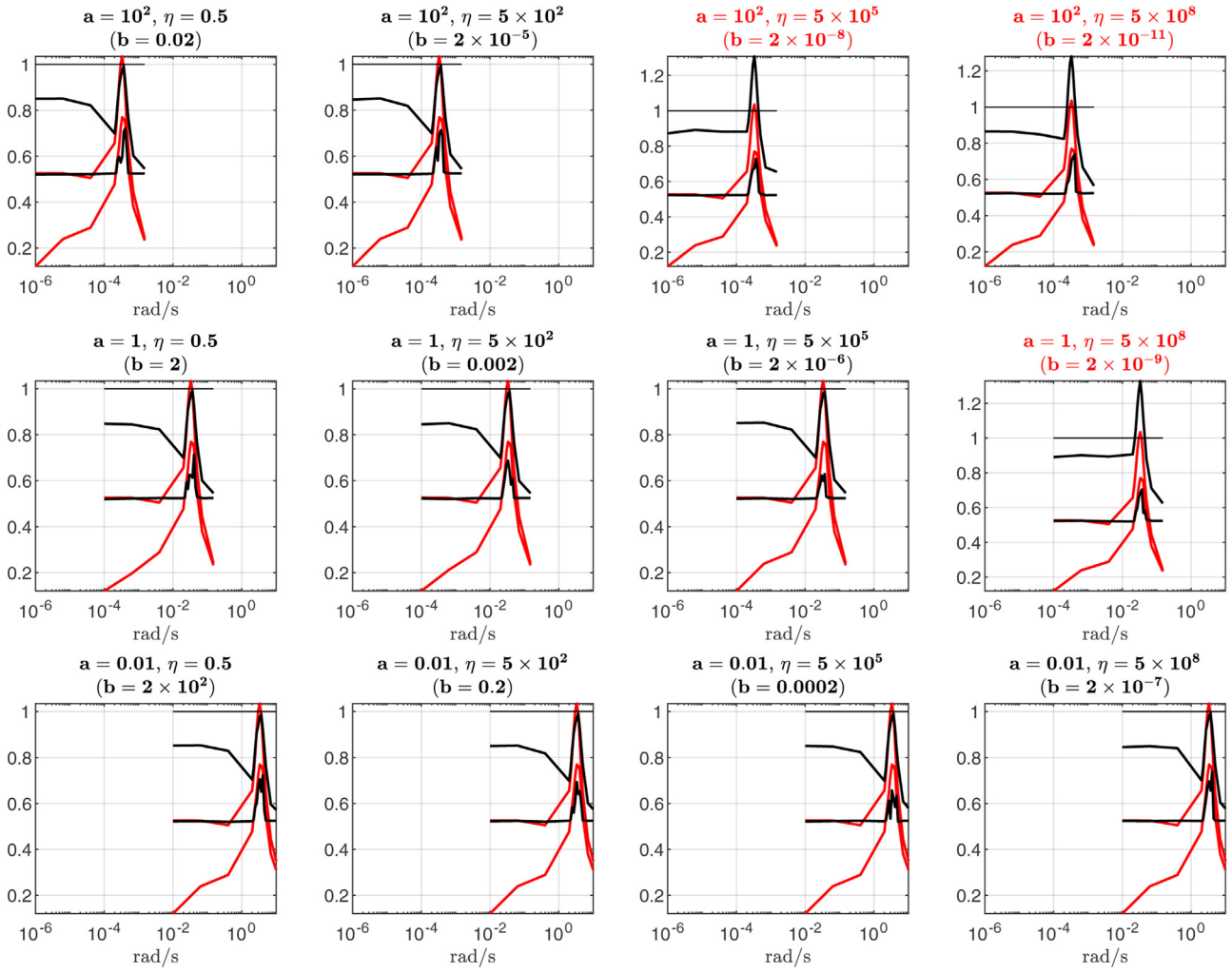

Fig. 11. Robustness analysis for variations on scaling parameters $a^{-1}\gamma_j$, $a^{-1}k_j$ and η. The bounds with ME, in black, are invariant for the changes in scale, except for cases where $b \leq 10^{-7}$. With FE (in red) the results are independent of the parameterisation. The variation in a shifts the response in frequency, but the bounds remain very similar.

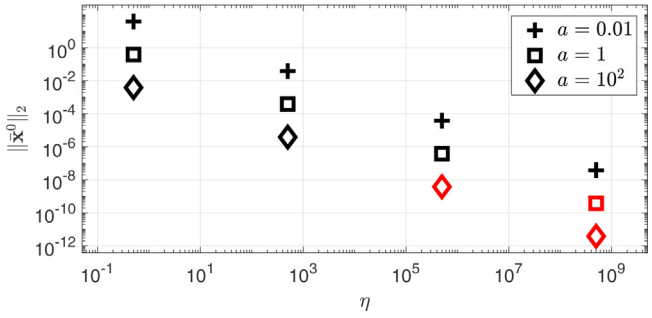

Fig. 12. Norm of the nominal equilibrium for variations on scaling parameters $a^{-1}\gamma_j$, $a^{-1}k_j$ and η. In red are the cases $(a\eta)^{-1} = b < 10^{-7}$.

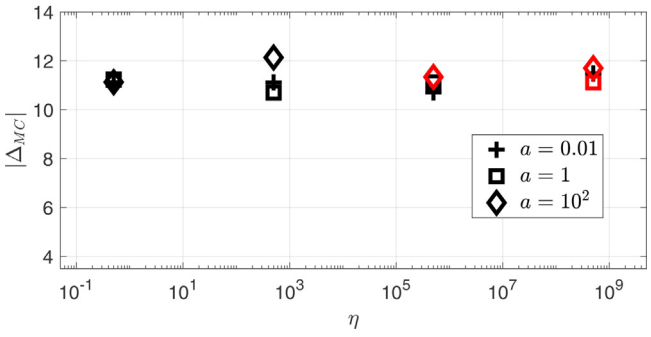

Fig. 13. Destabilising $|\Delta_{II}|$ found for variations on scaling parameters $a^{-1}\gamma_j$, $a^{-1}k_j$ and η. They are close for every variation of parameters, including for $(a\eta)^{-1} = b < 10^{-7}$ (in red).

and analysis of the CRN from the scaled parameters used for implementation. In fact, scaling can be used to avoid numerical issues, by carrying out the controller design and performing the robustness analysis with possibly unfeasible but numerically balanced parameterisations, before finally scaling the systems appropriately for DSD implementation.

6. Conclusions

We have demonstrated how robust stability analysis based on the structured singular value technique can be applied to the CRN representation of a biomolecular linear feedback system. We showed that it is critical to address the nonlinearities resulting from the use of chemical reactions, and to operate within the natural

coordinates of the CRN, accounting for the positivity of the system and the movement of its equilibrium due to uncertainty.

Our results indicate that it is possible to provide highly accurate guarantees on robustness for such systems by applying μ-analysis on the linearisation of the nonlinear dynamics. Although the use of μ-analysis around a fixed equilibrium is computationally cheaper, it provides a conservative uncertainty bound, thus underestimating the level of uncertainty for which the closed-loop system remains stable. Improving the linearisation model with a moving equilibrium produced robustness results that showed better agreement with the behaviour of the nonlinear system. Use of formal robustness analysis methods based on μ was shown to provide more reliable results than sampling-based methods such as Monte Carlo campaigns and testing vertices of the parameter space.

Finally, we showed how the analysis of the CRN can be decoupled from the parameterisation used to ensure a feasible implementation using nucleic acid-based chemistry, since existing scaling procedures preserve the robustness of the original CRN.

Acknowledgements

DGB acknowledges funding from the University of Warwick, the EPSRC/BBSRC Centre for Doctoral Training in Synthetic Biology via grant EP/L016494/1 and the BBSRC/EPSRC Warwick Integrative Synthetic Biology Centre via grant BB/M017982/1.

References

[1] R. Daniel, J.R. Rubens, R. Sarpeshkar, T.K. Lu, Synthetic analog computation in living cells, Nature 497 (7451) (2013) 619–623.
[2] A.W.K. Harris, J.A. Dolan, C.L. Kelly, J. Anderson, A. Papachristodoulou, Designing genetic feedback controllers, IEEE Trans. Biomed. Circuits Syst. 9 (4) (2015) 475–484.
[3] F. Fages, G. Le Guludec, O. Bournez, A. Pouly, Strong turing completeness of continuous chemical reaction networks and compilation of mixed analog-digital programs, in: K.H. J. Feret (Ed.), Computational Methods in Systems Biology, Vol. 10545 of Lecture Notes in Computer Science, Springer, Cham, 2017, pp. 108–127.
[4] R. Brijder, Computing with chemical reaction networks: a tutorial, Nat. Comput. (2018) 1–19.
[5] H.J. Buisman, H.M.M. ten Eikelder, P.A.J. Hilbers, A.M.L. Liekens, Computing algebraic functions with biochemical reaction networks, Artif. Life 15 (1) (2008) 5–19.
[6] S.A. Salehi, K.K. Parhi, M.D. Riedel, Chemical reaction networks for computing polynomials, ACS Synth. Biol. 6 (1) (2017) 76–83.
[7] M. Vasic, D. Soloveichik, S. Khurshid, CRN++: Molecular programming language, in: D. Doty, H. Dietz (Eds.), DNA Computing and Molecular Programming, Vol. 11145 of Theoretical Computer Science and General Issues, Springer International Publishing, 2018, pp. 1–18.
[8] K. Oishi, E. Klavins, Biomolecular implementation of linear I/O systems, IET Syst. Biol. 5 (4) (2011) 252–260.
[9] C. Cosentino, R. Ambrosino, M. Ariola, M. Bilotta, A. Pironti, F. Amato, On the realization of an embedded subtractor module for the control of chemical reaction networks, IEEE Trans. Autom. Control 61 (11) (2016) 3638–3643.
[10] H.-L. Chen, D. Doty, D. Soloveichik, Rate-independent computation in continuous chemical reaction networks, Proceedings of the 5th Conference on Innovations in Theoretical Computer Science (2014) 313–326, ACM.
[11] R. Shah, D. Del Vecchio, Signaling architectures that transmit unidirectional information despite retroactivity, Biophys. J. 113 (3) (2017) 728–742.
[12] M. Bilotta, C. Cosentino, A. Merola, D.G. Bates, F. Amato, Zero-retroactivity subtraction module for embedded feedback control of chemical reaction networks, IFAC-PapersOnLine 49 (26) (2016) 128–133.
[13] T.Y. Chiu, H.J.K. Chiang, R.Y. Huang, J.H.R. Jiang, F. Fages, Synthesizing configurable biochemical implementation of linear systems from their transfer function specifications, PLoS One 10 (9) (2015) e0137442.
[14] D. Soloveichik, G. Seelig, E. Winfree, DNA as a universal substrate for chemical kinetics, Proc. Natl. Acad. Sci. USA 107 (12) (2010) 5393–5398.
[15] N. Srinivas, J. Parkin, G. Seelig, E. Winfree, D. Soloveichik, Enzyme-free nucleic acid dynamical systems, Science 358 (6369) (2017), eaal2052.
[16] Y.-J. Chen, N. Dalchau, N. Srinivas, A. Phillips, L. Cardelli, D. Soloveichik, G. Seelig, Programmable chemical controllers made from DNA, Nat. Nanotechnol. 8 (10) (2013) 755–762.
[17] B. Yordanov, J. Kim, R.L. Petersen, A. Shudy, V.V. Kulkarni, A. Phillips, Computational design of nucleic acid feedback control circuits, ACS Synth. Biol. 3 (8) (2014) 600–616.
[18] L. Qian, E. Winfree, Scaling up digital circuit computation with DNA strand displacement cascades, Science 332 (6034) (2011) 1196–1201.
[19] R. Sawlekar, F. Montefusco, V.V. Kulkarni, D.G. Bates, Implementing nonlinear feedback controllers using DNA strand displacement reactions, IEEE Trans. Nanobioscience 15 (5) (2016) 443–454.
[20] M. Foo, J. Kim, R. Sawlekar, D.G. Bates, Design of an embedded inverse-feedforward biomolecular tracking controller for enzymatic reaction processes, Comput. Chem. Eng. 99 (2017) 145–157.
[21] N.M.G. Paulino, M. Foo, J. Kim, D.G. Bates, Uncertainty modelling and stability robustness analysis of nucleic acid-based feedback control systems, Proceedings of the 57th IEEE Conference on Decision and Control, Florida (2018) 1077–1082.
[22] S. Streif, K.-K.K. Kim, P. Rumschinski, M. Kishida, D.E. Shen, R. Findeisen, R.D. Braatz, Robustness analysis, prediction, and estimation for uncertain biochemical networks: an overview, J. Process Control 42 (2016) 14–34.
[23] P. Psarris, C.A. Floudas, Robust stability analysis of systems with real parametric uncertainty: A global optimization approach, Int. J. Robust Nonlinear Control 5 (8) (1995) 699–717.
[24] J. Doyle, Analysis of feedback systems with structured uncertainties, IEE Proc. D Control Theory and Appl. 129 (6) (1982) 242–250.
[25] S. Skogestad, I. Postlethwaite, Multivariable Feedback Control: Analysis and Design, 2nd Edition, John Wiley, New York, 2005.
[26] J. Doyle, A. Packard, K. Zhou, Review of LFTs, LMIs, and mu, Proceedings of the 30th IEEE Conference on Decision and Control (1991) 1227–1232.
[27] L. Andersson, A. Rantzer, Robustness of equilibria in nonlinear systems, IFAC Proc. 32 (2) (1999) 2256–2261.
[28] M. Kishida, R.D. Braatz, On the analysis of the eigenvalues of uncertain matrices by μ and ν: applications to bifurcation avoidance and convergence rates, IEEE Trans. Autom. Control 61 (3) (2016) 748–753.
[29] P. Tóth, J. Érdi, Mathematical models of chemical reactions: Theory and Applications of Deterministic and Stochastic Models, Manchester University Press, 1989.
[30] M. Foo, R. Sawlekar, D.G. Bates, Exploiting the dynamic properties of covalent modification cycle for the design of synthetic analog biomolecular circuitry, J. Biol. Eng. 10 (1) (2016) 15.
[31] L. Farina, S. Rinaldi, Positive Linear Systems: Theory and Applications, Wiley, New York, 2000.
[32] H. Khalil, Nonlinear control, in: Global Edition, Pearson Education Limited, Essex, England, 2015.
[33] J.X. Zhang, J.Z. Fang, W. Duan, L.R. Wu, A.W. Zhang, N. Dalchau, B. Yordanov, R. Petersen, A. Phillips, D.Y. Zhang, Predicting DNA hybridization kinetics from sequence, Nat. Chem. 10 (1) (2018) 91–98.
[34] G. Balas, R. Chiang, A. Packard, M. Safonov, Robust Control Toolbox™, User's Guide, The Math Works, Inc, Natick, Massachusetts, United States, 2018 March, r2018a Edition.
[35] C. Zou, X. Wei, Q. Zhang, Y. Liu, Synchronization of chemical reaction networks based on DNA strand displacement circuits, IEEE Access 6 (2018) 20584–20595.